JOURNAL OF SCIENCE & ENGINEERING, MAY, 1967. VOL IV PP. 87~118

Analysis and Discussion on Stability of Flow in Open Channels for Various Shapes of Cross Sections

(各種不同斷面之渠道穩定分析及其研討)

By

Chih-Wu Ho

(何 智 武)

CONTENTS

*** This study was supported by the National Council on Science Development in 1966 (July, 1966-June, 1967).

** Instructor of Fluid Mechanics and Engineering Mathematics, Department of Civil Engineering, Chung-Hsing University.

SYNOPSIS

A series of charts have been derived by Francis F. Escoffier and Marden B. Boyd in Nov. 1962,(1)* to assist in the design of rectangular, trapezoidal (with side slopes of 1:1 1:2 and 1:3), and circular channels.

They adopted three simple derived parameters in these charts: one a function of channel discharge and base width; another, a function of the depth of flow and the base width; and a third, a function of the channel slope, roughness, and base width. In the case of a circular channel, the base width is replaced with the diameter. Each of the charts is divided into three zones, representing tranquil flow, steady-rapid flow, and pulsating flow. The last zone of flow represents channels in which roll waves are apt to form.

At the suggestion of Prandtl, Kirschmer explained that the effect of channel shape may be due to the development of secondary flow, which is apparently more pronounced in square-cornered sections than modified rounded sections. A high secondary flow involves high energy loss and thus accounts for high channel resistance. From this point of view, the author of this paper is intended to develop a series of charts of such rounded regular shapes of sections (involving parabolic section) for design purpose. Besides, the chart of trapezoidal section with side slope $1:\frac{\sqrt{3}}{3}$ (the best hydraulic section) is also derived in order to compare with one of the three other slopes which have been derived by Escoffier and Boyd.

At the end of this paper, with those rounded and unrounded shapes of cross sections, a series of discussions and comparisons are made on its stability for flow conditions and the effect among those various geometric conditions or shapes.

I. Introduction

This paper is concerned with an analytical procedure based on the Manning formula. This procedure is of particular value because it defines the transition from tranquil flow to rapid flow and also from steady flow to pulsating flow by means of three relatively simple parameters which have been explained in the synopsis.

Rectilinear plots using these derived parameters resulting in charts of those round-cornered sections are useful to the designer concerned with open-channel flow problems. These charts are considered to be an inprovement over other methods because they graphically show the relationship between several types of flow and because only one chart is required to define the flow conditions that can occur in a channnel of specific geometry. The development of the analytical procedure for defining several types of open-channel flow are described. The procedure is

---

* The number in the bracket denotes the number of the references in the end of this paper.

adapted to a graphical solution for open-channel flow problems in which criteria for tranquil, rapid and pulsating flows are combined in a single chart.

The four shapes of cross sections, with top width T and depth y which will be derived in this paper are sketched as follows;

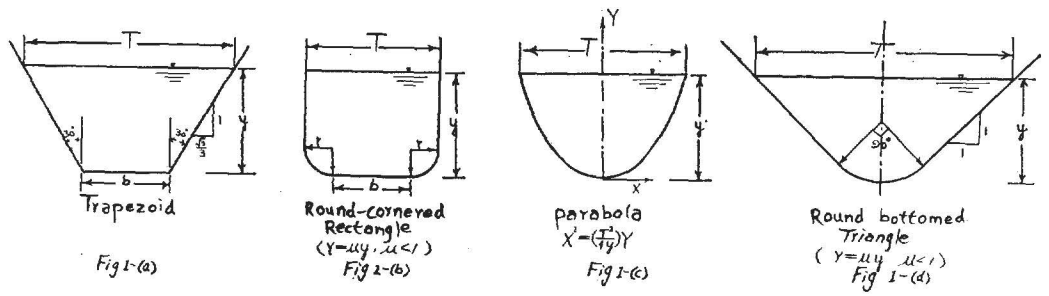

Four design charts will be derived from the above four sections separately. Including the three charts which has been derived by Escoffier and Boyd, there would be seven design charts with both rounded and unrounded sections. A thorough discussion among the square-cornered and the round-cornered rectangles, the parabola and the round-bottomed triangle are made separately on its stability for flow conditions. A comparison between the best trapezoidal section and the section of side slopes "1 : 1", are made in order to watch out the efficiency between the best hydraulic section and the others.

II. Notation and Description

The following symbols are adopted for use in this paper:

A = cross-sectional area of channel section, in square feet;
b = bottom width in rectangular or trapezoidal sections and diameter in circular section, in feet;
C = critical velocity or celerity of a gravity wave, in feet/sec;
D = hydraulic depth or mean depth, in feet;
F = Froude number;
g = gravitational acceleration, in feet per second per second;
n = Manning roughness coefficient;
P = wetted perimeter, in feet;
Q = discharge, in cubic feet per second;
R = hydraulic radius, in feet;
r = the radius of the rounded corner in the rounded sections, in feet;
S = slope of channel bottom;
t = time, in second;
V = mean velocity in channel section, in feet per second;
V_0 = normal velocity in channel section, in feet per second;
T = width at water surface, in feet;
x = distance along channel measured in down stream direction, in feet;

y = depth above lowest point in channel section, in feet;

w = stage variable.

The related derived parameters are as follows:

$\zeta=\frac{y}{b}$; $\rho=\frac{R}{b}$, $\delta=\frac{D}{b}$, $\alpha=\frac{A}{b^2}$ (no dimensions), $\xi=\frac{Q}{b^{\frac{5}{2}}}$ (dimensions: $L^{\frac{1}{2}}t^{-1}$). $J=\frac{S^{\frac{1}{2}}b^{\frac{1}{6}}}{n}$

III. Geometrical Consideration for the Four Chanuel Shapes

In theoretical development, we assume that the open-channel resistance is properly expressed by the Manning formula:

$$V_0=\frac{1.486}{n}S^{\frac{1}{2}}R^{\frac{2}{3}} \quad \cdots\cdots(1)$$

Hence, the discharge Q can be represented as:

$$Q=AV_0=\frac{1.486}{n}AS^{\frac{1}{2}}R^{\frac{2}{3}} \quad \cdots\cdots(2)$$

Each symbol in the above equations can be found in Sec. II.

We now introduce the four parameters:

$$\rho=\frac{R}{b}, \quad \alpha=\frac{A}{b^2}, \quad J=\frac{S^{\frac{1}{2}}b^{\frac{1}{6}}}{n} \quad \text{and} \quad \xi=\frac{Q}{b^{\frac{5}{2}}},$$

and from these, the Manning formula can be written as:

$$V_0=\frac{1.486}{n}S^{\frac{1}{2}}R^{\frac{2}{3}}=1.486\cdot\frac{S^{\frac{1}{2}}b^{\frac{1}{6}}}{n}\cdot b^{\frac{1}{2}}\cdot\frac{R^{\frac{2}{3}}}{b^{\frac{2}{3}}} \quad \cdots\cdots(3)$$

$$\text{or} \quad V_0=1.486J\,b^{\frac{1}{2}}\rho^{\frac{2}{3}} \quad \cdots\cdots(3)'$$

From Eq. (2), $$\frac{Q}{b^{\frac{5}{2}}}=1.486\frac{S^{\frac{1}{2}}b^{\frac{1}{6}}}{n}\cdot\frac{A}{b^2}\cdot\frac{R^{\frac{2}{3}}}{b^{\frac{2}{3}}} \quad \cdots\cdots(4)$$

$$\text{or} \quad \xi=(1.486\alpha\rho^{\frac{2}{3}})J \quad \cdots\cdots(4)'$$

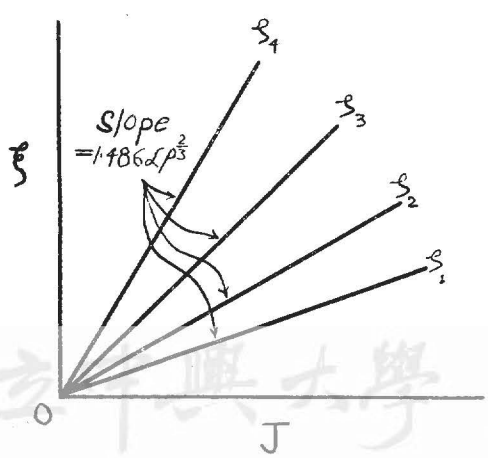

Fig 2

Eq. (4)′ is the most foundamental equation and will be used for constructing the basic graphs on the design charts. For various channel shapes, the parameters α and ρ are both functions of another parameter ζ. Therefore, for a particular channel section and a given value of ζ, all values of J and ξ will lie on a straight line passing through the origin and with slope $1.486\alpha\rho^{\frac{2}{3}}$. The slope of the line will vary for ζ-values as illustrated in Fig. 2. above.

The functional relations between each of the three parameters α, ρ and σ with ζ for the four shapes of sections as in Fig. 1—(a), (b), (c), and (d) will now be derived[2].

(a) Trapezoidal section (with side slope $1:\frac{\sqrt{3}}{3}$ for each side):

Refer to Fig. 1—(a),

$$T=b+\frac{2\sqrt{3}}{3}y=b+\frac{2\sqrt{3}}{3}\left(\frac{y}{b}\right)b=b\left(1+\frac{2\sqrt{3}}{3}\zeta\right)\cdots\cdots(5\text{—a})$$

$$A=\tfrac{1}{2}y(b+T)=y\left(b+\frac{\sqrt{3}}{3}y\right)=b^2\zeta\left(1+\frac{\sqrt{3}}{3}\zeta\right)\cdots\cdots(5\text{—b})$$

$$P=b+2\sqrt{y^2+\tfrac{1}{3}y^2}=b\left(1+2\zeta\cdot\frac{2}{\sqrt{3}}\right)=b\left(1+\frac{4\sqrt{3}}{3}\zeta\right)\cdots\cdots(5\text{—c})$$

$$\alpha=\frac{A}{b^2}=\frac{b^2\zeta\left(1+\frac{\sqrt{3}}{3}\zeta\right)}{b^2}=\zeta\left(1+\frac{\sqrt{3}}{3}\zeta\right)\cdots\cdots(5\text{—d})$$

$$\rho=\frac{R}{b}=\frac{A}{bp}=\frac{b^2\zeta\left(1+\frac{\sqrt{3}}{3}\zeta\right)}{b^2\left(1+\frac{4\sqrt{3}}{3}\zeta\right)}=\zeta\left(\frac{3+\sqrt{3}\zeta}{3+4\sqrt{3}\zeta}\right)\cdots\cdots(5\text{—e})$$

$$\delta=\frac{D}{b}=\frac{A}{bT}=\frac{b^2\zeta\left(1+\frac{\sqrt{3}}{3}\zeta\right)}{b^2\left(1+\frac{2\sqrt{3}}{3}\zeta\right)}=\zeta\left(\frac{3+\sqrt{3}\zeta}{3+2\sqrt{3}\zeta}\right)\cdots\cdots(5\text{—f})$$

(b) Round-cornered Rectangle. ($r=\mu y$, $\mu<1$):

Refer to Fig. 1—(b),

$$T=b+2r=b+2\mu y=b(1+2\mu\zeta)\cdots\cdots(6\text{—a})$$

$$A=Ty-2r^2+\frac{1}{2}\pi r^2=Ty-\left(2-\frac{\pi}{2}\right)r^2$$

$$=b(1+2\mu\zeta)y-0.43\mu^2y^2=b^2\zeta[1+(2-0.43\mu)\mu\zeta]\cdots\cdots(6\text{—b})$$

$$P=2(y-r)+b+\pi r=b[1+(2+1.14\mu)\zeta]\cdots\cdots(6\text{—c})$$

$$\alpha=\frac{A}{b^2}=\zeta[1+(2-0.43\mu)\mu\zeta]\cdots\cdots(6\text{—d})$$

$$\rho=\frac{R}{b}=\frac{A}{bp}=\zeta\left[\frac{1+(2-0.43\mu)\mu\zeta}{1+(2+1.14\mu)\zeta}\right]\cdots\cdots(6\text{—e})$$

$$\delta=\frac{D}{b}=\frac{A}{bT}=\zeta\left[\frac{1+(2-0.43\mu)\mu\zeta}{1+2\mu\zeta}\right]\cdots\cdots(6\text{—f})$$

(c) Parabola (the base width b is replaced with the top width T.):

Refer to Fig. 1—(c),

$$T=b\cdots\cdots(7\text{—a})$$

$$A=\tfrac{2}{3}Ty=\tfrac{2}{3}by=\tfrac{2}{3}b^2\zeta\cdots\cdots(7\text{—b})$$

$$P=2\int_c ds=2\int_0^{\frac{1}{2}T}\sqrt{1+\left(\frac{dY}{dX}\right)^2}dX=2\int_0^{\frac{1}{2}T}\sqrt{1+\left(\frac{8y}{T^2}\right)^2X^2}dX$$

$$=\left(\frac{T^2}{8y}\right)\left[\sqrt{1+\left(\frac{8y}{T^2}X\right)^2}\left(\frac{8g}{T^2}X\right)+\ln\left(\sqrt{1+\left(\frac{8y}{T^2}X\right)^2}+\frac{8y}{T^2}X\right)\right]_0^{\frac{T}{2}}$$

$$=\frac{1}{2}\sqrt{b^2+16y^2}+\frac{b^2}{8y}\ln\left(\frac{\sqrt{b^2+16y^2}+4y}{b}\right)$$

$$=\frac{b}{2}[\sqrt{1+16\zeta^2}+\frac{1}{4\zeta}\ln(\sqrt{1+16\zeta^2}+4\zeta)] \quad \cdots\cdots (7-c)$$

$$\alpha=\frac{A}{b^2}=\frac{2}{3}\zeta \quad \cdots\cdots (7-d)$$

$$\rho=\frac{A}{bP}=\frac{\frac{2}{3}b^2\zeta}{\frac{1}{2}b^2[\sqrt{1+16\zeta^2}+\frac{1}{4\zeta}\ln(\sqrt{1+16\zeta^2}+4\zeta)]}$$

$$=\frac{4}{3}\zeta\left[\frac{4\zeta}{4\zeta\sqrt{1+16\zeta^2}+\ln(\sqrt{1+16\zeta^2}+4\zeta)}\right] \quad \cdots\cdots (7-e)$$

$$\delta=\frac{A}{bT}=\alpha=\frac{A}{b^2}=\frac{2}{3}\zeta \quad \cdots\cdots (7-f)$$

(d) Round-bottomed Triangle (with side slope 1 : 1 for each side, radius $r=\mu y$, $\mu<1$, and the base width is also replaced with the top width T.):
Refer to Fig. 1—(d),

$$T=b. \quad \cdots\cdots (8-a)$$

$$A=\frac{b^2}{4}-r^2\left(1-\frac{\pi}{4}\right)=\frac{b^2}{4}-0.21\mu^2y^2=b^2(0.25-0.21\mu^2\zeta^2) \quad \cdots\cdots (8-b)$$

$$P=\sqrt{2}b-\left(2-\frac{\pi}{2}\right)r=\sqrt{2}b-0.43\mu y=b(1.41-0.43\mu\zeta) \quad \cdots\cdots (8-c)$$

$$\alpha=\frac{A}{b^2}=0.25-0.21\mu^2\zeta^2 \quad \cdots\cdots (8-d)$$

$$\rho=\frac{A}{bP}=\frac{0.25-0.21\mu^2\zeta^2}{1.41-0.43\mu\zeta} \quad \cdots\cdots (8-e)$$

$$\delta=\frac{A}{bT}=\alpha=0.25-0.21\mu^2\zeta^2 \quad \cdots\cdots (8-f)$$

IV. Critical Depth Curves and Pulsating Flow Curves.

The transition from tranguil flow to rapid flow occurs when the normal velocity V_0 equals the critical velocity C. But the critical velocity is represented by

$$C=\sqrt{gD} \quad \cdots\cdots (9)$$

Hence, from Eq.(1),

$$V_0=\frac{1.486}{n}S^{\frac{1}{2}}R^{\frac{2}{3}}=\sqrt{gD},$$

or

$$\frac{S^{\frac{1}{2}}}{n}=\frac{\sqrt{gD}}{1.486\,R^{\frac{2}{3}}} \quad \cdots\cdots (10)$$

Eq. (10) can also be rewritten as

$$\frac{S^{\frac{1}{2}}b^{\frac{1}{6}}}{n}=\frac{\nu g\cdot\sqrt{\frac{D}{b}}}{1.486\left(\frac{R^{\frac{2}{3}}}{b^{\frac{2}{3}}}\right)} \quad \cdots\cdots (11)$$

or $$J_c=3.816\frac{\delta^{\frac{1}{2}}}{\rho^{\frac{2}{3}}} \quad \cdots\cdots (11)'$$

in which the subscript C denotes critical. Since ρ and δ are functions of ζ, the value of J_c can be computed for any desired channel shape and for each given ζ-value to locate the transition point.

Computation of J_c-values for a number of ζ-values will define the critical depth curve which marks the transition from tranquil to steady-rapid flow.

The derivation of equations in the following section (sect.V) that defines the conditions under which waves of instability are likely to develop is essentially as presented by Escoffier.[3] In this derivation, it is assumed that there exists a uniform distribution of velocity in the channel cross section. Escoffier represented a similar derivation for the case of nonuniform distribution of velocity in the channel cross section.[4] Consideration of uniform velocity distribution in the section results in a more conservative equation defining the pulsating flow curve.

V. Equations of Characteristics

In open-channel flow, the dynamic and the continuity equations[5] for a uniform channel which governing the flow are:

$$\frac{\partial V}{\partial t}+V\frac{\partial V}{\partial x}+g\frac{\partial y}{\partial x}=gS\left(1-\frac{V^2}{V_0^2}\right) \quad \cdots\cdots (12)$$

and $$T\frac{\partial y}{\partial t}+A\frac{\partial V}{\partial x}+VT\frac{\partial y}{\partial x}=0 \quad \cdots\cdots (13)$$

where the symbols V, t, x, y, T and S are all noted as in section II If we multiply Eq.(13) by a parameter λ and then plus Eq.(12), we obtain

$$\frac{\partial V}{\partial t}+(V+\lambda A)\frac{\partial V}{\partial x}+\lambda T\frac{\partial y}{\partial t}+(g+\lambda VT)\frac{\partial y}{\partial x}=gS\left(1-\frac{V^2}{V_0^2}\right) \quad \cdots\cdots (14)$$

The condition for the left side of Eq. (14) to be directional derivative[6][7] in (x, t) plane is

$$\frac{1}{V+\lambda A}=\frac{\lambda T}{g+\lambda VT} \quad \cdots\cdots (16)$$

or $$\lambda=\pm\sqrt{\frac{g}{TA}} \quad \cdots\cdots (16)'$$

Substituting Eq. (16)' into Eq. (14), we get

$$\frac{\partial V}{\partial t}+\left(V\pm\sqrt{\frac{gA}{T}}\right)\frac{\partial V}{\partial x}\pm\sqrt{\frac{gT}{A}}\left(\frac{\partial y}{\partial t}\right)+\left(g\pm\sqrt{\frac{gT}{A}}\cdot V\right)\frac{\partial y}{\partial x}=gS\left(1-\frac{V^2}{V_0^2}\right) \quad \cdots (17)$$

or $$\frac{\partial V}{\partial t}+\left(V\pm\sqrt{\frac{gA}{T}}\right)\frac{\partial V}{\partial x}\pm\left[\sqrt{\frac{gT}{A}}\frac{\partial y}{\partial t}+\left(\pm\sqrt{\frac{gA}{T}}+V\right)\sqrt{\frac{gT}{A}}\frac{\partial y}{\partial x}\right]=gS\left(1-\frac{V^2}{V_0^2}\right) \quad (17)'$$

But $c=\sqrt{gD}=\sqrt{\frac{gA}{T}}$, and a new variable, stage variable w is now introduced to replace y as a measure of the level of water in the channel, thus.

$$w=\int_0^A C\frac{dA}{A}=\int_0^y\sqrt{\frac{gA}{T}}\frac{Tdy}{A}=\int_0^y\sqrt{\frac{gT}{A}}\,dy \quad \cdots\cdots (18)$$

and $$\frac{\partial w}{\partial x}=\sqrt{\frac{gT}{A}}\frac{\partial y}{\partial x};\quad \frac{\partial w}{\partial t}=\sqrt{\frac{gT}{A}}\frac{\partial y}{\partial t} \quad \cdots\cdots (19)$$

Using these expressions, Eq. (17)′ becomes

$$\frac{\partial V}{\partial t}+(V\pm C)\frac{\partial V}{\partial x}\pm\left[\frac{\partial w}{\partial t}+(V\pm C)\frac{\partial w}{\partial t}\right]=gS\left(1-\frac{V^2}{V_0^2}\right) \quad \cdots\cdots (20)$$

Put $$U=V\pm w \quad \cdots\cdots (21)$$

where V and w are both functions of t and x, then

$$\frac{\partial U}{\partial t}=\frac{\partial V}{\partial t}\pm\frac{\partial w}{\partial t};\quad \frac{\partial U}{\partial x}=\frac{\partial V}{\partial x}\pm\frac{\partial w}{\partial x} \quad \cdots\cdots (22)$$

Substituting Eqs.(22) into Eq. (20), then it may be simplified as

$$\frac{\partial U}{\partial t}+(V\pm C)\frac{\partial U}{\partial x}=gS\left(1-\frac{V^2}{V_0^2}\right) \quad \cdots\cdots (23)$$

By using chain rule, we have

$$\frac{\partial U}{\partial t}=\frac{dU}{dt}-\frac{\partial U}{\partial x}\frac{dx}{dt} \quad \cdots\cdots (24)$$

From this, Eq. (23) may also be expressed as

$$\frac{dU}{dt}-\left[\frac{dx}{dt}-(V\pm C)\right]\frac{\partial U}{\partial x}=gS\left(1-\frac{V^2}{V_0^2}\right) \quad \cdots\cdots (25)$$

in which, $\frac{\partial U}{\partial t}$ are eliminated.

In order to eliminate the expression in the bracket in Eq. (25), we define an equation, which along the path in the (x, t) plane to be $dx=(V\pm C)dt$ ……(26)

then Eq. (25) becomes

$$dU=gS\left(1-\frac{V^2}{V_0^2}\right)dt \quad \cdots\cdots (27)$$

or $$d(V\pm w)=gS\left(1-\frac{V^2}{V_0^2}\right)dt \quad \cdots\cdots (28)$$

Eqs. (26) and (28) are the equations of characteristics.

VI. Interpretation of Equations——Instability Criteria

In Eq. (26), the upper (plus) sign represents a pulse or wave point traveling downstream with a velocity V+C and will be designated as a forward characteristic. Whereas, the lower (minus) sign represents a pulse or wave point traveling with a velocity V−C, moving upstream or downstream depending on the relative magnitude of V and C, and will be designated as a backward characteristic.

Now, we observe that for the case of uniform flow in which $V=V_0$, the small change in $\frac{dU}{dt}$ can be derived as follow for the small variations $\triangle V$, $\triangle V_0$ and $\triangle W$:

$$\triangle\left[gS(1-\frac{V^2}{V_0^2})\right]=-gS\left(\frac{2V_0^2V\cdot\triangle V-2V^2\cdot V_0\cdot\triangle V_0}{V_0^4}\right)=\frac{2gS}{V}(\triangle V_0-\triangle V)\cdots(29)$$

From which, we conclude that, along the forward characteristic

$$d(\triangle V+\triangle w)=\frac{2gS}{V}(\triangle V_0-\triangle V)dt \quad\cdots\cdots(30)$$

and along the backward characteristic

$$d(\triangle V-\triangle w)=\frac{2gS}{V}(\triangle V_0-\triangle V)dt \quad\cdots\cdots(31)$$

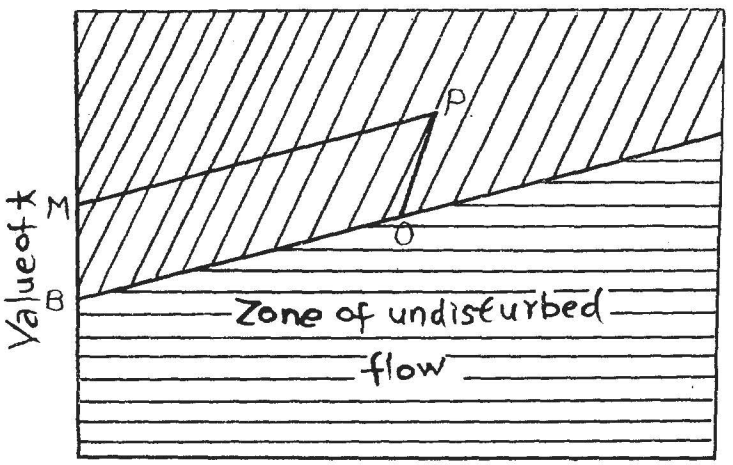

Fig 3

In Fig. 3, the lines MP and BO(positive slope)represent forward characteristics and the line OP (negative slope) a backward characteristic. The zone to the right of BO is assumed to be undisturbed uniform flow. A pulse or disturbance begins at M and moves downstream along MP.

In general, the effect of channel friction will be to reduce the magnitude of this pulse as it moves downstream, but in the case of steep channels, the opposite may be true and the pulse will continue to increase in magnitude. In such a case, the flow is called unstable.

Next, we demonstrate instability criteria. In order to eliminate $\triangle V$, we consider the line OP in Fig. 3 to be very short, so that the right side of Eq.(31) to be negligible, then, $\triangle V-\triangle w=0$ ……(32)

From this, Eq. (30) becomes

$$d\triangle w=\frac{gS}{V_0}(\triangle V_0-\triangle w)dt \quad\cdots\cdots(33)$$

Noting that, V_0 is a function of w, it is possible to write

$$\triangle V_0=\frac{dV_0}{dw}\triangle w \quad\cdots\cdots(34)$$

Substituting Eq. (34) into Eq. (33), then

$$d(\triangle w)=\frac{gS}{V_0}\left(\frac{dV_0}{dw}-1\right)\triangle w\,dt \quad\cdots\cdots(35)$$

Let us now discuss Eq. (35) in three possible cases:

(a) If $\frac{dV_0}{dw} > 1$, then $d(\triangle w) > 0$, or $\triangle w$ increases. In this case, the function of waves of instability along the forward characteristic.

(b) If $-1 < \frac{dV_0}{dw} < 1$, then $d(\triangle w) < 0$, or $\triangle w$ decreases. In this interval, the flow will be steady.

(c) If $\frac{dV_0}{dw} < -1$, (the companion formula of $\frac{dV_0}{dw} > 1$), instability occur along the backward characteristic. It requires the normal velocity V_0 to decrease as the stage variable w increases. This is an unusual condition that is met in a closed conduit flowing nearly full.

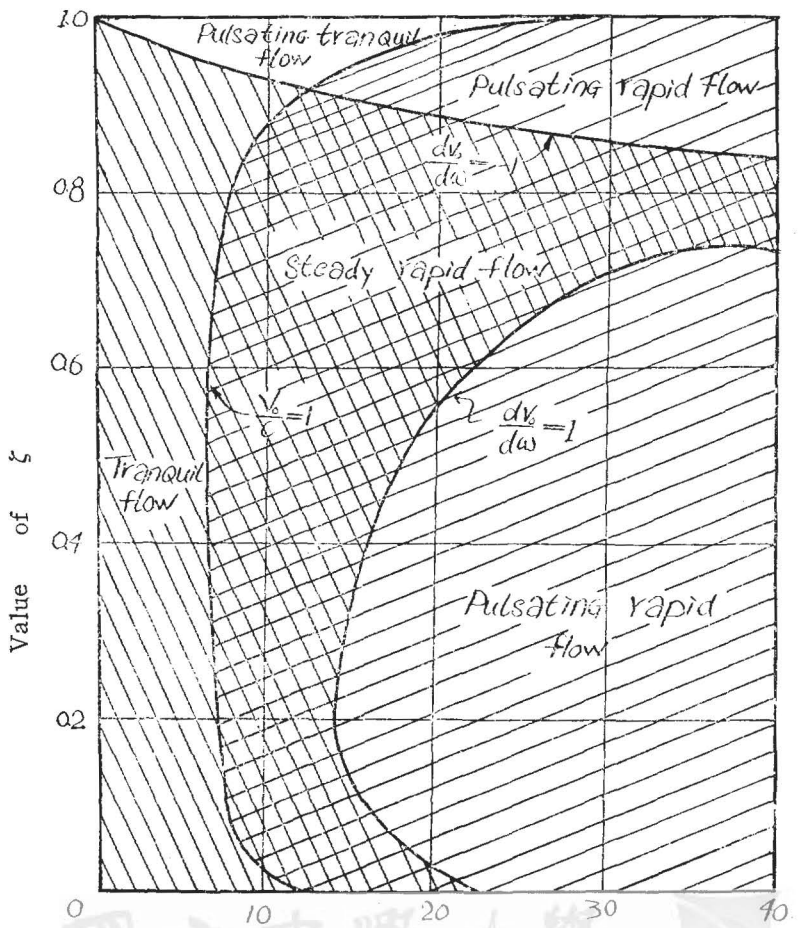

Fig. 4

As an illustrative example, Escffier and Boyd gave a ζ-J diagram (Fig.4) for illustrating several types of flow that may occur in a circular section.

In this diagram, there are three curves: $\frac{dV_0}{dw}=1$, $\frac{dV_0}{dw}=-1$, and $\frac{V_0}{C}=1$(critical flow curve). The right side of curve $\frac{V_0}{C}=1$ (represents rapid flow region and the left side, tranquil flow region. The region between curves $\frac{dV_0}{dw}=1$ and $\frac{dV_0}{dw}=-1$ is steady and the other two parts are the pulsating flow regions. Frow above classification, the diagram can be divided into four different flow parts, namely; tranquil, pulsating tranquil, steady rapid, and pulsating rapid, as shown in Fig. 4.

The transition from steady flow to pulsating flow occurs when

$$\frac{dV_0}{dw}=\pm 1 \quad \cdots\cdots(36)$$

From Eq. (3)', we take the derivative V_0 with respect to ρ yields

$$dV_0=\left(\frac{2}{3}\right)1.486b^{\frac{1}{2}}\rho^{-\frac{2}{3}}d\rho \quad \cdots\cdots(37)$$

and from Eq. (18), $dw=C\frac{dA}{A}=\sqrt{gD}\,\frac{Tdy}{A}=\sqrt{\frac{g}{D}}dy \quad \cdots\cdots(38)$

By the definition of ζ, $y=b\zeta$ or $dy=bd\zeta \quad \cdots\cdots(39)$

then, substituting (39) into (38), we get

$$dw=\sqrt{\frac{g}{D}}bd\zeta \quad \text{or} \quad dw=\sqrt{\frac{gb}{\delta}}d\zeta \quad \cdots\cdots(40)$$

since $\delta=\frac{D}{b}$

From Eqs. (37) and (40)

$$\frac{dV_0}{dw}=\frac{2}{3}\,\frac{1.486}{\sqrt{g}}\,\frac{J\delta^{\frac{1}{2}}}{\rho^{\frac{1}{3}}}\,\frac{d\rho}{d\zeta} \quad \cdots\cdots(41)$$

and also compare with Eq. (36), we get the following result.

$$\frac{2}{3}\,\frac{1.486}{\sqrt{g}}\,\frac{J\delta^{\frac{1}{2}}}{\rho^{\frac{1}{3}}}\,\frac{d\rho}{d\zeta}=\pm 1 \quad \cdots\cdots(42)$$

or $$J_i=\pm 5.723\,\frac{\rho^{\frac{1}{3}}}{\delta^{\frac{1}{2}}}\,\frac{d\zeta}{d\rho} \quad \cdots\cdots(43)$$

where the subscript i refers to the transition part.

The actual numerical computation of approximate J_i-values for a number of ζ-values will define the pulsating flow curve which marks the transition from steady flow to pulsating flow in various ζ-J charts.

VII Development and Use of Design Charts (Inclusion of Four Shapes)

The formulas which have been derived in the previous articles and will be used in constructing design charts are listed as follows:

$$\xi=1.486\alpha\rho^{\frac{2}{3}}J \quad \cdots\cdots(4)'$$

$$J_c=3.816\frac{\delta^{\frac{1}{2}}}{\rho^{\frac{2}{3}}} \qquad \cdots\cdots(11)'$$

$$J_1=\pm 5.723\frac{\rho^{\frac{1}{3}}}{\delta^{\frac{1}{2}}}\frac{d\zeta}{d\rho} \qquad \cdots\cdots(43)$$

with these three formulas and the parameters α, ρ and δ all (in terms of ζ)of the four different sections, we would now develop the design charts (ξ-J diagram) separately for the sections of trapezoid, round-cornered rectangle, parabola and round-bottomed triangle. Computations required for these charts were made with a desk calculator and slide rule using a $\triangle\zeta$-increment of 0.004

(a) Trapezoidal Section (with side slope $1:\frac{\sqrt{3}}{3}$ for each side).

Referring to Eqs. (5—a) to (5—f), we obtain the following results.

$$\alpha=\zeta\left(1+\frac{\sqrt{3}}{3}\zeta\right)=\zeta+0.58\zeta^2$$

$$\rho=\zeta\left(\frac{3+\sqrt{3}\zeta}{3+4\sqrt{3}\zeta}\right)=\zeta-\frac{5.2\zeta^2}{3+6.93\zeta}$$

$$\delta=\zeta\left(\frac{3+\sqrt{3}\zeta}{3+2\sqrt{3}\zeta}\right)=\zeta-\frac{1.73\zeta^2}{3+3.46\zeta}$$

$$\frac{d\rho}{d\zeta}=\frac{9+10.4\zeta+13\zeta^2}{(3+6.93\zeta)^2}\quad,\qquad \frac{d\zeta}{d\rho}=\frac{(3+6.93\zeta)^2}{9+10.4\zeta+13\zeta^2}$$

$$\xi=\left[1.486(\zeta+0.58\zeta^2)\left(\zeta-\frac{5.2\zeta^2}{3+6.93\zeta}\right)^{\frac{2}{3}}\right]J,$$

$$J_c=3,816\cdot\frac{\left(\zeta-\frac{1.73\zeta^2}{3+3.46\zeta}\right)^{\frac{1}{2}}}{\left(\zeta-\frac{5.2\zeta^2}{3+6.93\zeta}\right)^{\frac{2}{3}}}$$

$$J_1=\pm 5,723\cdot\frac{\left(\zeta-\frac{5.2\zeta^2}{3+6.93\zeta}\right)^{\frac{1}{3}}}{\left(\zeta-\frac{1.73\zeta^2}{3+3.46\zeta}\right)^{\frac{1}{2}}}\cdot\frac{(3+6.93\zeta)^2}{9+10.4\zeta+13\zeta^2}$$

The design chart (Fig. 5) of this section was obtained by using above expressions with ζ-values ranging from 0.02 to 0.98

(b) Round-cornered Rectangle ($r=\mu y$, $\mu<1$)

Referring to Eqs.(6—a)to(6—f), and further assuming $\mu=\frac{1}{4}$ (the most possible case), we get the following results.

$$\alpha=\zeta\left[1+(2-0.43\cdot\tfrac{1}{4})\cdot\tfrac{1}{4}\zeta\right]=\zeta+0.47\zeta^2$$

$$\rho=\zeta\left[\frac{1+(2-0.43\cdot\frac{1}{4})\cdot\frac{1}{4}\zeta}{1+(2+1.14\cdot\frac{1}{4})\zeta}\right]=\frac{\zeta+0.47\zeta^2}{1+2.29\zeta}$$

$$\delta=\zeta\left[\frac{1+(2-0.43\cdot\frac{1}{4})\cdot\frac{1}{4}\zeta}{1+2(\frac{1}{4})\zeta}\right]=\frac{\zeta+0.47\zeta^2}{1+0.5\zeta}$$

$$\frac{d\rho}{d\zeta}=\frac{1+0.94\zeta+1.08\zeta^2}{(1+2.29\zeta)^2}\quad,\qquad \frac{d\zeta}{d\rho}=\frac{(1+2.29\zeta)^2}{1+0.94\zeta+1.08\zeta^2}$$

$$\xi=\left[1.486(\zeta+0.47\zeta^2)\left(\frac{\zeta+0.47\zeta^2}{1+2.29\zeta}\right)^{\frac{2}{3}}\right]J$$

$$J_c=3,816\frac{\left(\frac{\zeta+0.47\zeta^2}{1+0.5\zeta}\right)^{\frac{1}{2}}}{\left(\frac{\zeta+0.47\zeta^2}{1+2.29\zeta}\right)^{\frac{2}{3}}}$$

$$J_1=\pm 5,723\cdot\frac{\left(\frac{\zeta+0.47\zeta^2}{1+2.29\zeta}\right)^{\frac{1}{3}}}{\left(\frac{\zeta+0.47\zeta^2}{1+0.5\zeta}\right)^{\frac{1}{2}}}\cdot\frac{(1+2.29\zeta)^2}{1+0.94\zeta+1.08\zeta^2}$$

The design chart with ζ-values ranging from 0.02 to 0.98 was plotted as shown in Fig. 6.

(c) Parabola. [2]

Referring to Eqs. (7—a) to (7—f), we have the following expressions:

$$\alpha=\tfrac{2}{3}\zeta=0.67\zeta$$

$$\rho=\frac{5.3\zeta^2}{4\zeta\sqrt{1+16\zeta^2}+\ln[\sqrt{1+16\zeta^2}+4\zeta]}\fallingdotseq\frac{5.3\zeta^2}{8\zeta(1+\frac{8}{3}\zeta^2)}=\frac{2\zeta}{3+8\zeta^2}$$

$$\delta=\tfrac{2}{3}\zeta=0.67\zeta$$

$$\frac{d\rho}{d\zeta}=\frac{2(3-8\zeta^2)}{(3+8\zeta^2)^2}\qquad\frac{d\zeta}{d\rho}=\frac{(3+8\zeta^2)^2}{2(3-8\zeta^2)}$$

$$\xi=1.486(\tfrac{2}{3}\zeta)\left[\frac{2\zeta}{3+8\zeta^2}\right]^{\frac{2}{3}}J=\left[1.57\zeta\left(\frac{\zeta}{3+8\zeta^2}\right)^{\frac{2}{3}}\right]J$$

$$J_c=3,816\frac{\left(\frac{2}{3}\zeta\right)^{\frac{1}{2}}}{\left(\frac{2\zeta}{3+8\zeta^2}\right)^{\frac{2}{3}}}=1.97\frac{\zeta^{\frac{1}{2}}}{\left(\frac{\zeta}{3+8\zeta^2}\right)^{\frac{2}{3}}}$$

$$J_1=\pm 5,723\frac{\left(\frac{2\zeta}{3+8\zeta^2}\right)^{\frac{1}{3}}}{\left(\frac{2}{3}\zeta\right)^{\frac{1}{2}}}\cdot\frac{d\zeta}{d\rho}=\pm 3.9\frac{(3+8\zeta^2)^{\frac{5}{3}}}{(3-8\zeta^2)\zeta^{\frac{1}{6}}}$$

The design chart with ζ-values varying from 0.02 to 1.58 was plotted as shown in Fig. 7.

(d) Round-bottomed Triangle. ($r=\mu y$, $\mu<1$, and with side slope 1:1 for each side).

Referring to Eqs, (8—a) to (8—f), and further assuming $\mu=\frac{1}{2}$ (the most possible case), we obtain the following results:

$$\alpha=0.25-0.21(\tfrac{1}{2})^2\zeta^2=0.25-0.05\zeta^2$$

$$\rho=\frac{0.25-0.21(\frac{1}{2})^2\zeta^2}{1.41-0.43(\frac{1}{2})\zeta}=\frac{0.25-.05\zeta^2}{1.41-0.22\zeta}$$

$$\delta=0.25-0.21(\tfrac{1}{2})^2\zeta^2=0.25-0.05\zeta^2$$

$$\frac{d\rho}{d\zeta}=\frac{0.06-0.14\zeta+0.01\zeta^2}{(1.41-0.22\zeta)^2},\qquad\frac{d\zeta}{d\rho}=\frac{(1.41-0.22\zeta)^2}{0.06-0.14\zeta+0.01\zeta^2}$$

$$\xi=1,486\alpha\rho^{\frac{2}{3}}J=\left[1,486(0.25-0.05\zeta^2)\left(\frac{0.25-0.05\zeta^2}{1.41-0.22\zeta}\right)^{\frac{2}{3}}\right]J$$

$$J_c=3,816\frac{(0.25-0.05\zeta^2)^{\frac{1}{2}}}{\left(\frac{0.25-0.05\zeta^2}{1.41-0.22\zeta}\right)^{\frac{2}{3}}}$$

$$J_1=\pm 5,723\frac{\left(\frac{0.25-0.05\zeta^2}{1.41-0.22\zeta}\right)^{\frac{1}{3}}}{(0.25-0.05\zeta^2)^{\frac{1}{2}}}\left[\frac{(1.41-0.22\zeta)^2}{0.06-0.14\zeta+0.01\zeta^2}\right]$$

The design chart with ζ-values varying from 0.02 to 0.50 was plotted as shown in Fig. 8.

The values of the four shapes for each parameter and of each ζ were computed and have been shown in Table 1. to 4. From these tables, the above four charts (Figs. 5~8) have been plotted.

In hydraulic design of open channels, the discharge of the channel may be determined first from hydraulic or hydrologic conditions, and then determine the proper channel shapes and assume the bottom widths. When we determine the proper shape of the channel, the design charts which have been derived above can be applied directly instead of miscellaneous computations.

The general procedure in an open channel design are listed as follows:

(I) Determine the discharge of the given channel first.

(II) Fix the invert slope normally by local terrain.

(III) Select a proper Manning coefficient n appropriate to the material in the channel bottom and sides.

(IV) Assume a proper bottom width.

(V) Compute the two parameters:

$$\xi = \frac{Q}{b^{\frac{5}{2}}} \quad \text{and} \quad J = \frac{S^{\frac{1}{2}} b^{\frac{1}{6}}}{n}$$

(VI) Plot the point on the appropriate design chart. The zone in which the point plots determines the hydraulic characteristics of the flow for these particular channel conditions.

(VII) Since $y = \zeta b$, the normal depth can be obtained.

(VIII) The critical depth can be obtained by drawing a horizontal line from the plotted point to the critical depth curve and taking the interpolated ζ-value and then use the equation $y = \zeta b$.

(IX) To examine whether the range which the point falls is desirable or not. The critical flow is unstable as uniform flow, since slight changes in energy may result in appreciable changes in the depth.[8] Depths of flow within 10% of critical flow are also apt to be unstable. Therefore, if the part falls within this range, redesign of the channel is recommended and if the point falls in the pulsating flow zone, a reduction in the bottom slope is indicated.

(X) A number of different combinations of channel shape, bottom width, and slope can easily be investigated in order to compare the economic or hydraulic advantages.

In consequence of comparison, the three design charts-trapezoidal (with side slope 1:1), rectangular and trapezoidal sections which have been derived and plotted by Escoffier and Boyd are copied in this paper as shown in Fig. 9, Fig. 10. and Fig. 11.

Seven derived and copied figures (Fig. 5~Fig. 11), with computed data (Table 1 ~Table 4) are shown as follows.

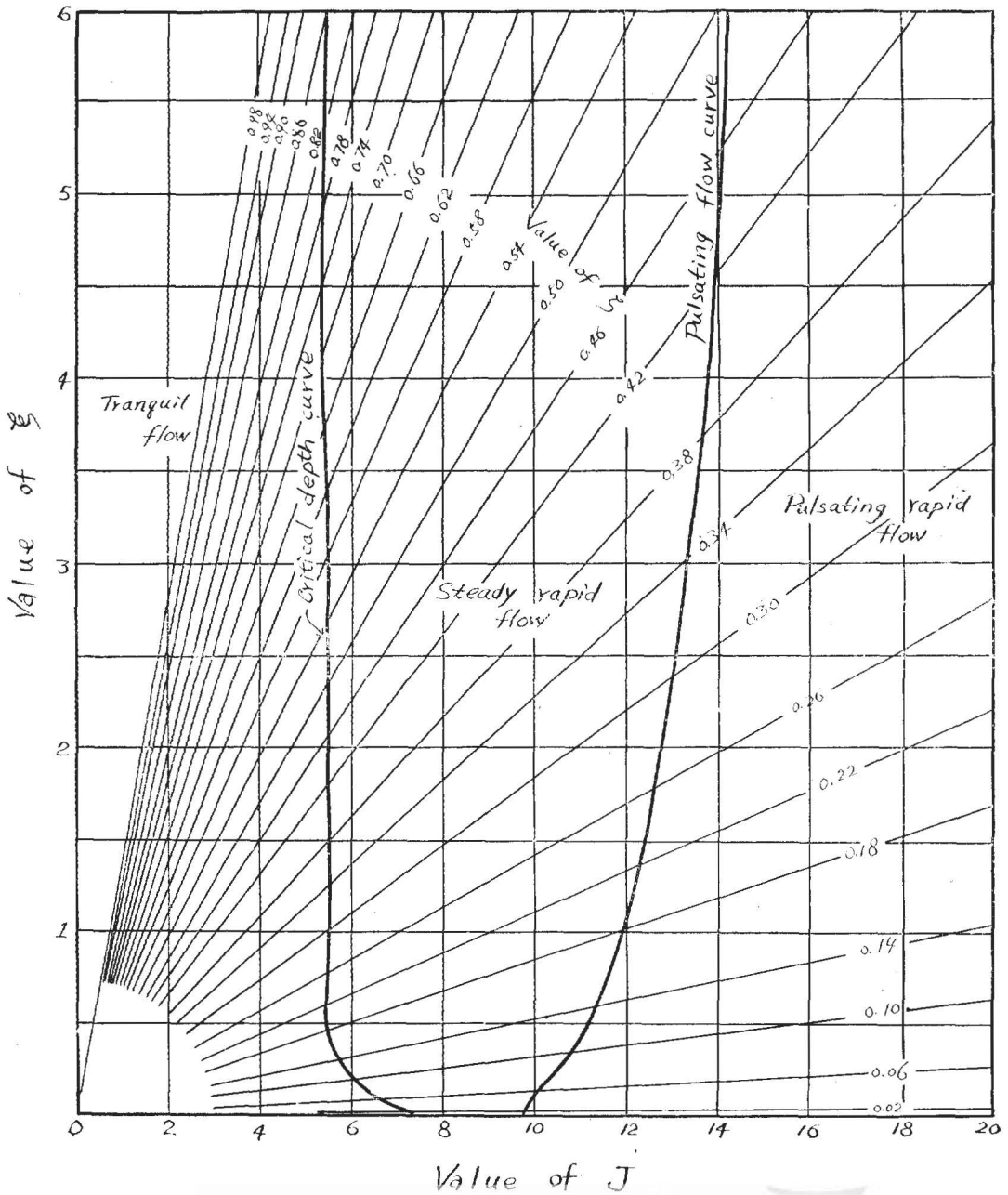

Fig. 5 Trapezoide (with side slope: $1:\frac{\sqrt{3}}{3}$)

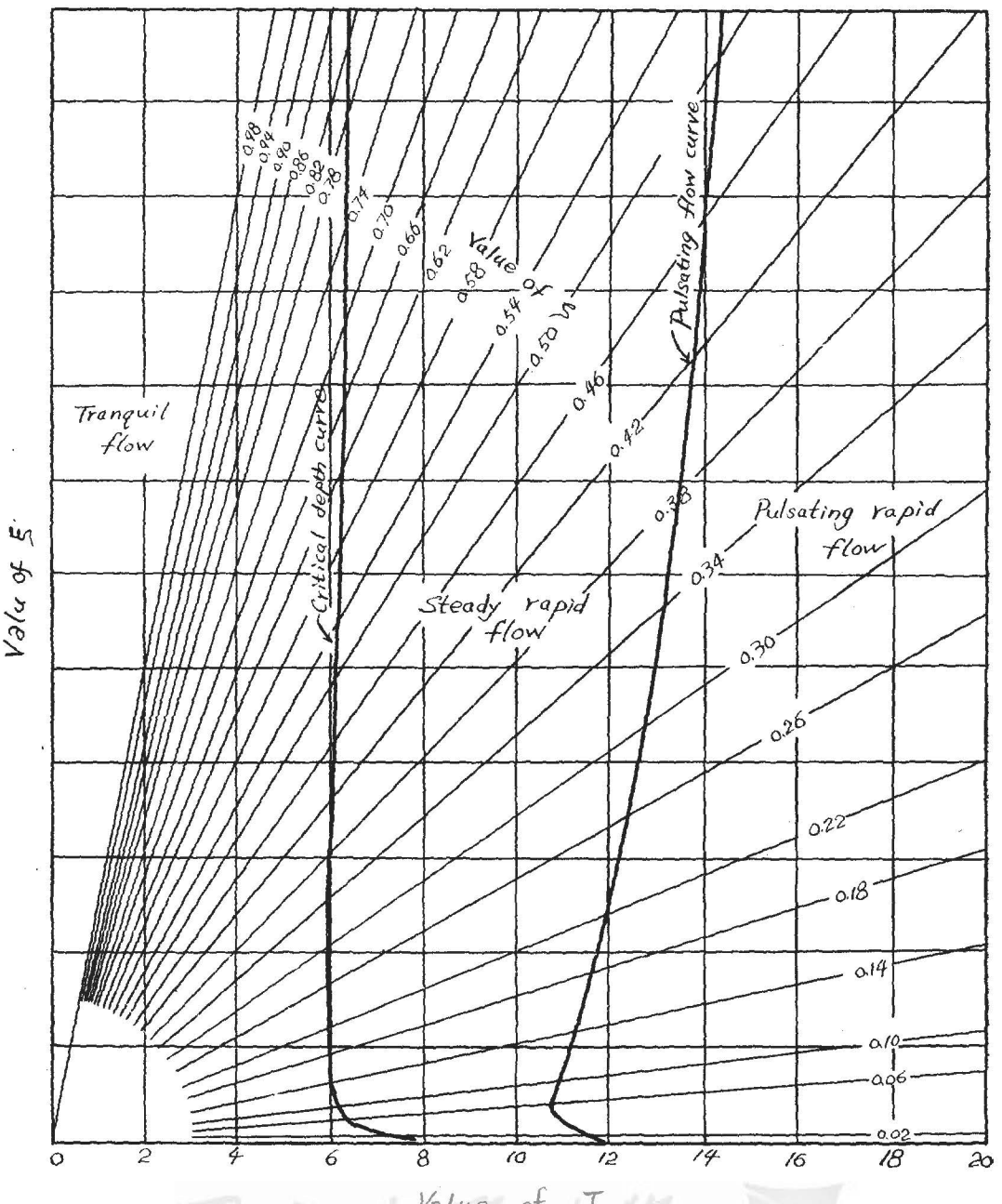

Fig 6. Round-cornered Rectangle. ($r = \mu y$, $\mu = \frac{1}{4}$)

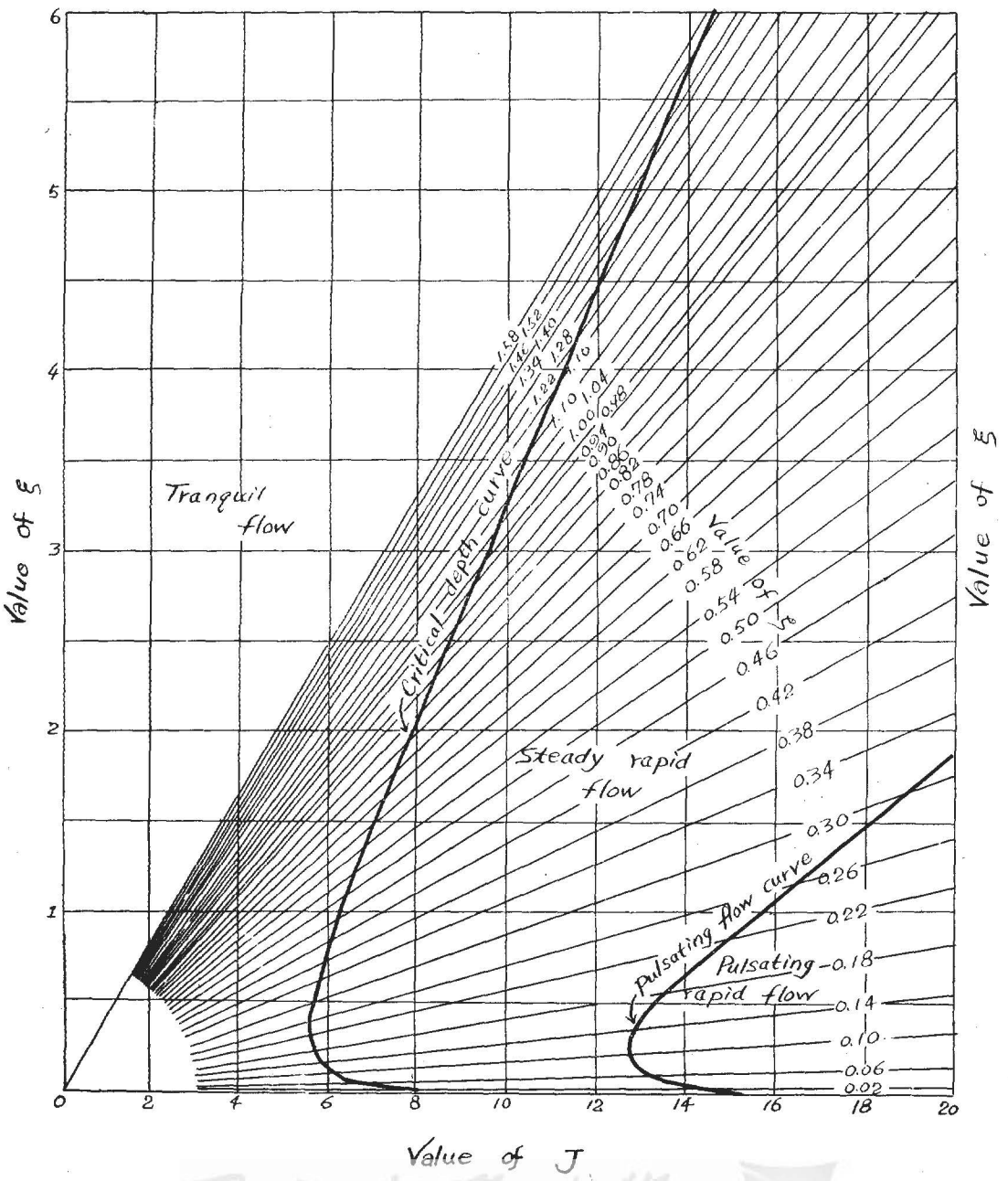

Fig. 7. Parabola (Equation: $X^2 = \frac{I^2}{4y} Y$)

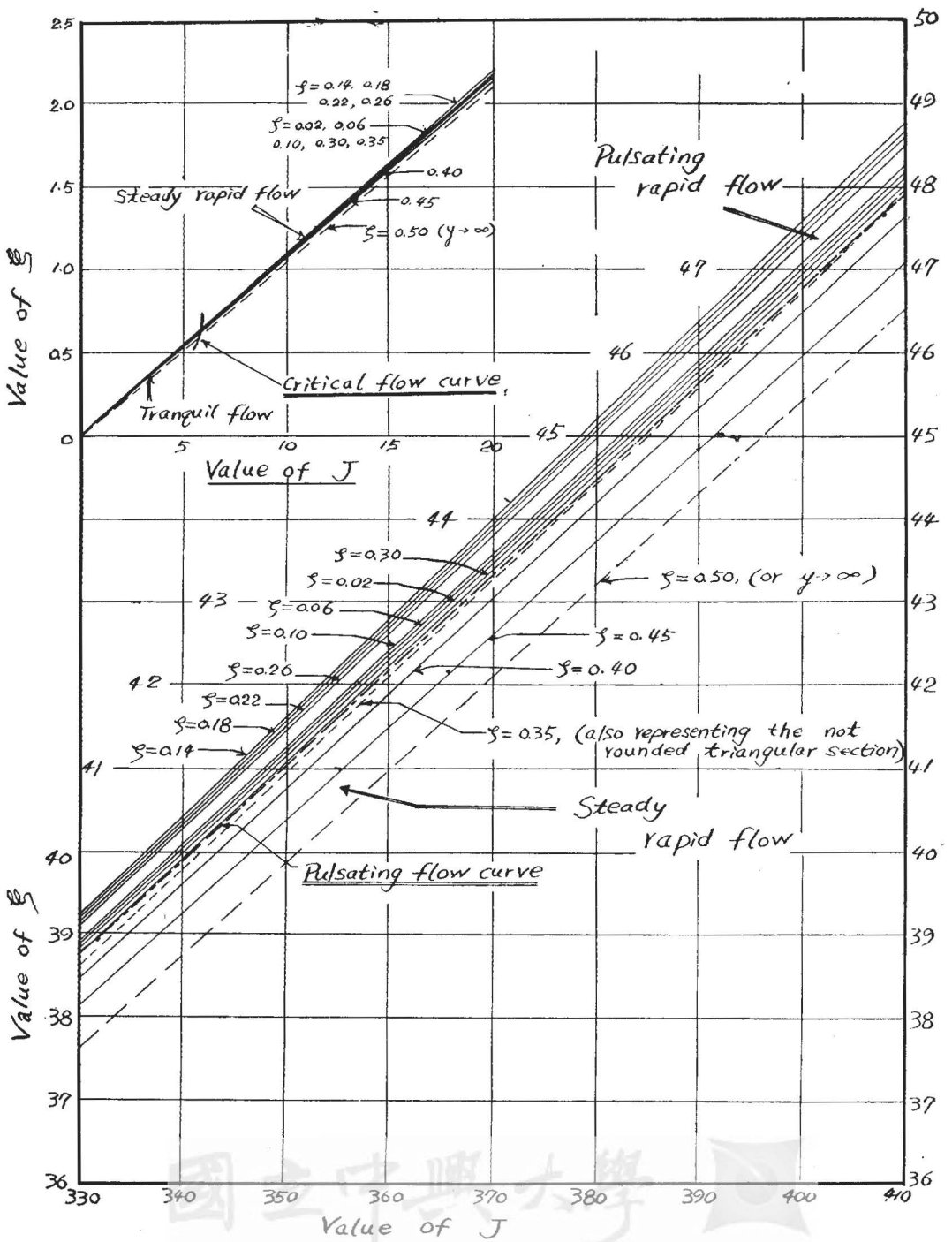

Fig. 8. Round-bottomed Triangle ($r=\mu y$, $\mu=\frac{1}{2}$)

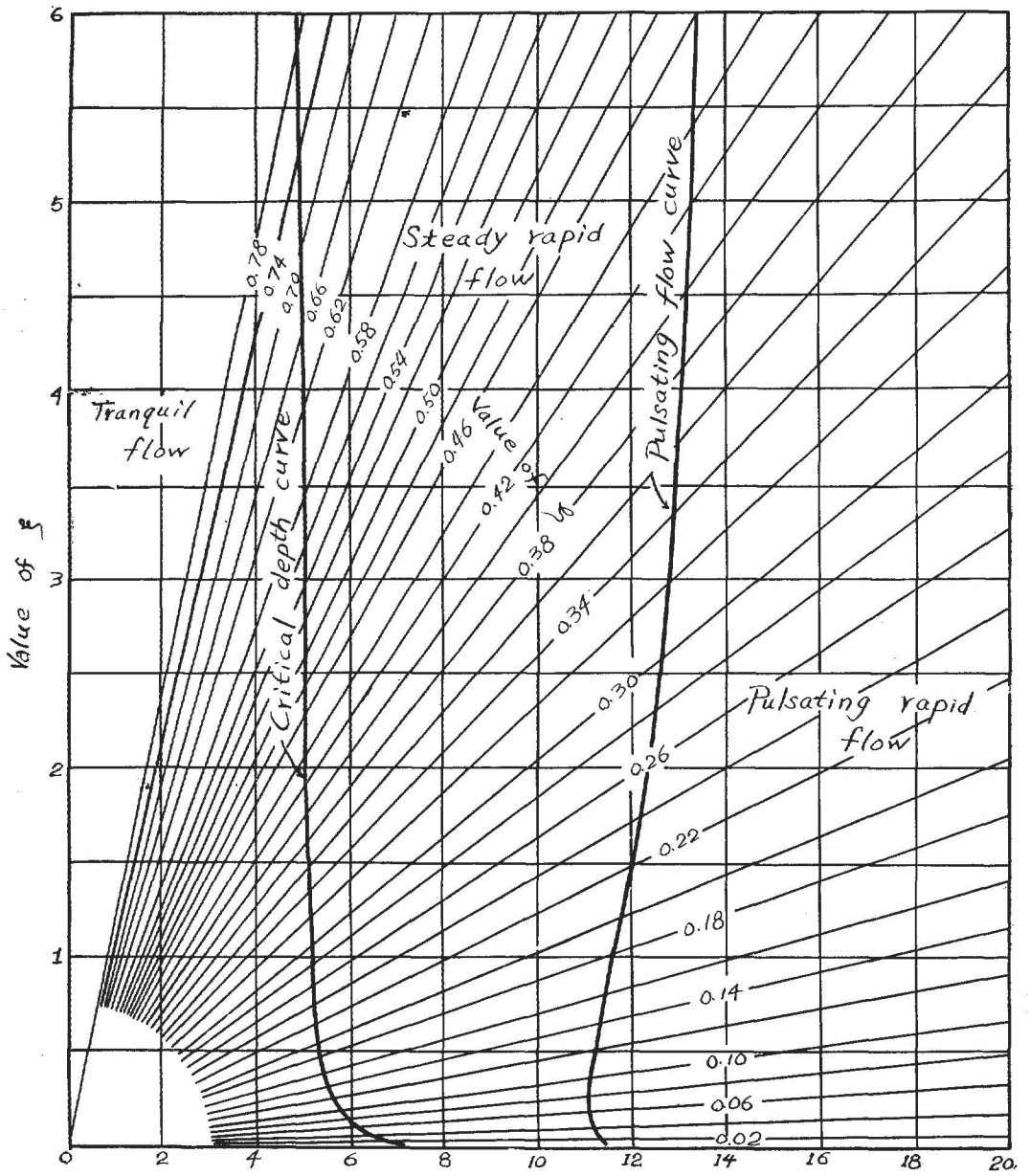

Fig. 9. Open-channel Flow for Trapezoidal Section
(with side slope; 1 on 1)

(Copied from Ref. Book No. 1.; plotted by Escoffier and Boyd.)

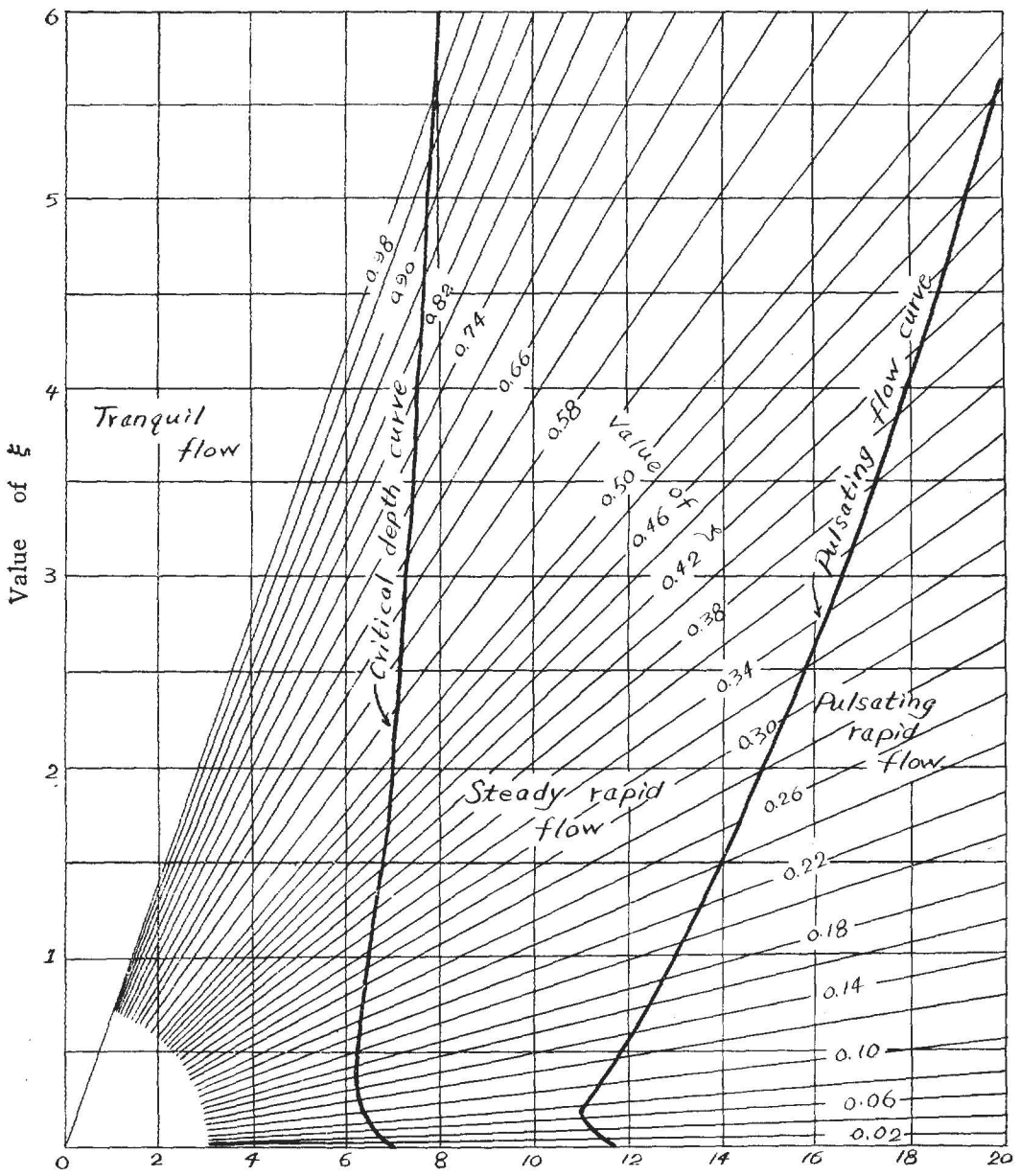

Fig 10. Open-channel Flow for Rectangular Section
(Copied from Ref. Book No. 1. ; plotted by Escoffier and Boyd.)

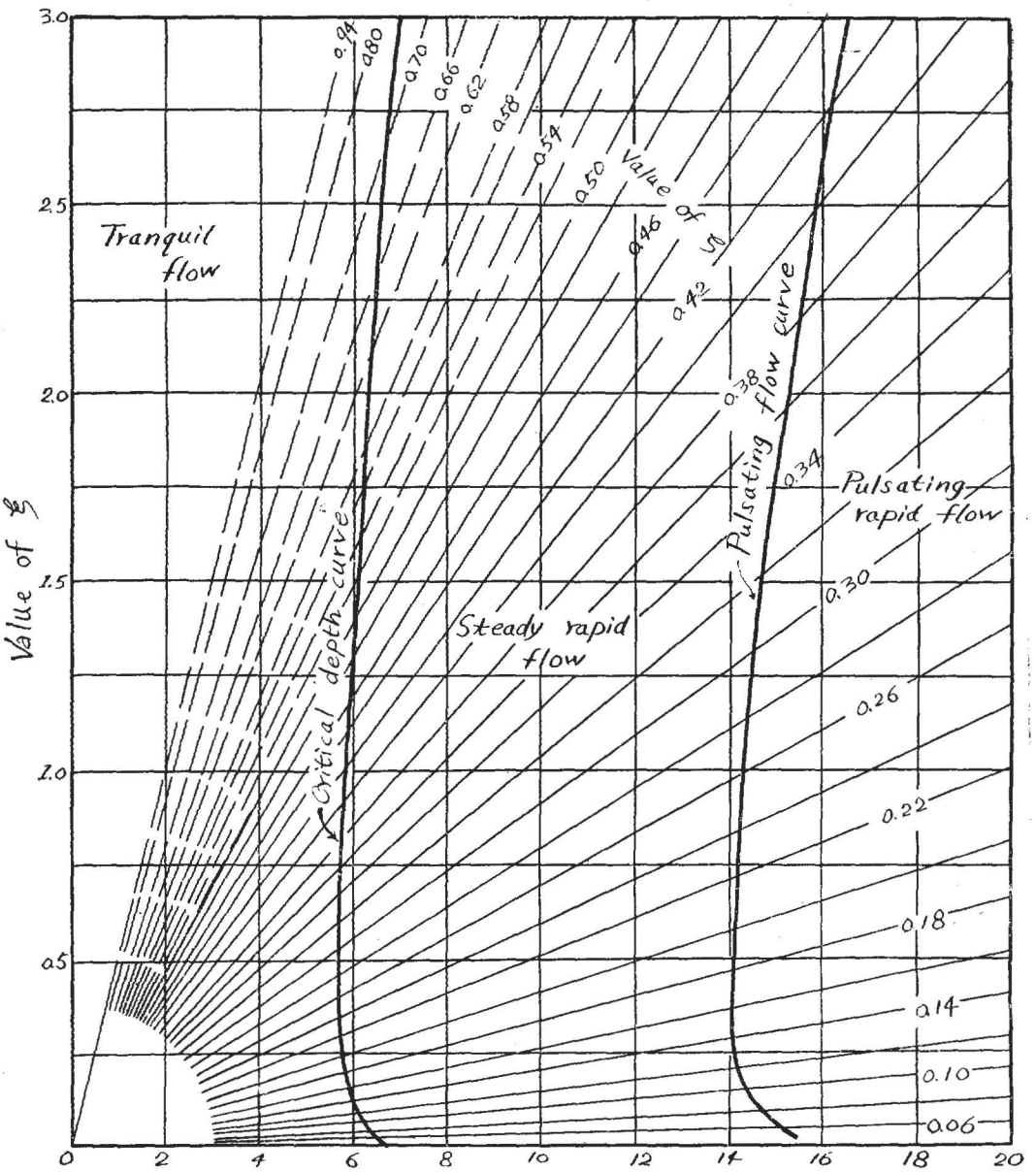

Fig. II Open-channel Flow for Circular Section
(Copied from Ref Book No.1; plotted by Escoffier and Boyd.)
{ ——— ξ line, lower semi-circle.
{ – – – – ξ line, upper semi-circle.

Table. 1. *Computed Data (Trapezoidal Section, Side slope* $\frac{\sqrt{3}}{3}$ *on* 1.)

(See Fig. 5)

ζ	α	ρ	δ	slope $=1.486\alpha\rho^{\frac{2}{3}}$	$J_c=3.816\frac{\delta^{\frac{1}{2}}}{\rho^{\frac{2}{3}}}$	$J_1=5.723\frac{\rho^{\frac{1}{3}}}{\delta^{\frac{1}{2}}}\frac{d\zeta}{d\rho}$
0.02	0.020	0.0194	0.020	0.0022	7.45	9.71
0.06	0.062	0.0567	0.058	0.0136	6.24	10.10
0.10	0.106	0.0860	0.095	0.0320	6.02	10.92
0.14	0.151	0.1150	0.130	0.0517	5.80	11.30
0.18	0.198	0.1504	0.165	0.0835	5.46	11.97
0.22	0.250	0.1600	0.198	0.1105	5.74	11.78
0.26	0.300	0.1900	0.230	0.1403	4.90	12.50
0.30	0.352	0.2080	0.261	0.1822	5.69	12.90
0.34	0.409	0.2275	0.292	0.2258	5.54	13.30
0.38	0.464	0.2470	0.322	0.2710	5.13	13.63
0.42	0.525	0.2650	0.351	0.3260	5.42	13.88
0.46	0.583	0.2820	0.380	0.3725	5.48	14.12
0.50	0.645	0.2990	0.409	0.4283	5.47	—
0.54	0.709	0.3150	0.437	0.4890	5.47	—
0.58	0.775	0.3310	0.464	0.5531	5.44	—
0.62	0.844	0.3460	0.490	0.6182	5.43	—
0.66	0.913	0.3610	0.518	0.6885	5.40	—
0.70	0.984	0.3800	0.540	0.7661	5.39	—
0.74	1.058	0.3900	0.570	0.8452	5.44	—
0.78	1.133	0.4037	0.390	0.9180	5.46	—
0.82	1.210	0.4090	0.600	0.9892	5.51	—
0.86	1.290	0.4300	0.740	1.0920	5.53	—
0.90	1.370	0.4500	0.670	1.1954	—	—
0.94	1.451	0.4570	0.070	1.2782	—	—
0.98	1.540	0.4700	0.072	1.4015	—	—

Table. 2. ***Computed Data (Round-cornered Rectangular Section)***

(See Fig. 6)

ζ	α	ρ	δ	slope$=1.486\alpha\rho^{\frac{2}{3}}$	$J_c=3.816\frac{\delta^{\frac{1}{2}}}{\rho^{\frac{2}{3}}}$	$J_1=5.723\frac{\rho^{\frac{1}{3}}}{\delta^{\frac{1}{2}}}\frac{d\zeta}{d\rho}$
0.02	0.020	0.019	0.022	0.002	7.48	11.74
0.06	0.077	0.071	0.075	0.019	6.04	10.70
0.10	0.102	0.085	0.101	0.030	6.20	10.95
0.14	0.149	0.113	0.140	0.052	6.03	11.28
0.18	0.195	0.138	0.179	0.078	6.00	11.63
0.22	0.242	0.162	0.221	0.102	6.04	11.91
0.26	0.291	0.181	0.260	0.139	6.07	12.28
0.30	0.342	0.203	0.298	0.173	6.00	12.80
0.34	0.395	0.222	0.337	0.216	5.98	13.17
0.38	0.448	0.239	0.381	0.256	6.07	13.32
0.42	0.503	0.256	0.416	0.303	6.05	13.73
0.46	0.559	0.272	0.454	0.349	6.08	13.93
0.50	0.618	0.288	0.494	0.399	6.12	14.21
0.54	0.677	0.302	0.533	0.445	6.15	—
0.58	0.738	0.315	0.573	0.509	6.22	—
0.62	0.801	0.334	0.612	0.571	6.18	—
0.66	0.865	0.343	0.652	0.627	6.21	—
0.70	0.930	0.355	0.691	0.692	6.28	—
0.74	0.997	0.371	0.727	0.763	6.25	—
0.78	1.066	0.382	0.767	0.834	6.30	—
0.82	1.136	0.394	0.804	0.911	6.34	—
0.86	1.210	0.408	0.850	0.989	6.34	—
0.90	1.281	0.419	0.883	1.070	6.37	—
0.94	1.355	0.432	0.923	1.149	6.43	—
0.98	1.430	0.451	0.973	1.262	6.34	—

Table. 3. *Computed Data (Parabolic Section)*

(See Fig. 7)

ζ	α	ρ	δ	slope$=1.486\alpha\rho^{\frac{2}{3}}$	$J=3.816\frac{\delta^{\frac{1}{2}}}{d^{\frac{2}{3}}}$	$J=5.723\frac{\rho^{\frac{1}{3}}}{\delta^{\frac{1}{2}}}\frac{d\zeta}{d\rho}$
0.02	0.013	0.013	0.013	0.001	8.21	14.92
0.06	0.041	0.040	0.041	0.007	6.61	13.33
0.10	0.074	0.065	0.074	0.016	6.10	12.82
0.14	0.093	0.089	0.093	0.028	5.82	12.90
0.18	0.122	0.111	0.122	0.041	5.72	13.52
0.22	0.152	0.132	0.152	0.056	5.72	14.82
0.26	0.170	0.151	0.170	0.070	5.62	16.50
0.30	0.202	0.160	0.202	0.088	5.77	18.62
0.34	0.226	0.173	0.226	0.105	5.84	22.43
0.38	0.254	0.183	0.254	0.122	5.94	26.60
0.42	0.282	0.190	0.282	0.138	6.08	33.80
0.46	0.306	0.196	0.306	0.154	6.22	45.21
0.50	0.333	0.200	0.333	0.169	6.42	63.04
0.54	0.360	0.202	0.360	0.184	6.61	107.11
0.58	0.386	0.204	0.386	0.502	6.80	251.17
0.62	0.413	0.204	0.413	0.212	7.04	—
0.66	0.444	0.202	0.444	0.226	7.31	—
0.70	0.474	0.200	0.474	0.237	7.60	—
0.74	0.492	0.204	0.492	0.251	7.78	—
0.78	0.520	0.198	0.520	0.262	8.05	—
0.82	0.545	0.196	0.545	0.276	8.33	—
0.86	0.572	0.193	0.572	0.284	8.65	—
0.90	0.605	0.190	0.605	0.294	8.91	—
0.94	0.627	0.187	0.627	0.306	9.24	—
0.98	0.654	0.182	0.654	0.309	9.65	—

Table. 4. *Computed Data. (Round-bottomed Triangular Section)*

(See Fig. 8)

ζ	α	ρ	δ	slope$=1.486\alpha\rho^{\frac{2}{3}}$	$J_c=3.816\frac{\delta^{\frac{1}{2}}}{\rho^{\frac{1}{3}}}$	$J=5.723\frac{\rho^{\frac{1}{3}}}{\delta^{\frac{1}{2}}}\frac{d\zeta}{d\rho}$
0.02	0.2500	0.1778	0.2500	0.1176	6.02	165.4
0.06	0.2498	0.1780	0.2498	0.1177	6.00	178.0
0.10	0.2495	0.1792	0.2495	0.1178	5.99	191.7
0.14	0.2490	0.1805	0.2490	0.1190	5.91	209.5
0.18	0.2480	0.1810	0.2480	0.1188	5.89	229.6
0.22	0.2476	0.1817	0.2476	0.1187	5.89	254.0
0.26	0.2466	0.1823	0.2466	0.1184	5.86	287.0
0.30	0.2455	0.1825	0.2455	0.1172	5.84	332.0
0.35	0.2440	0.1830	0.2440	0.1170	5.83	407.7
0.40	0.2420	0.1831	0.2420	0.1163	5.81	529.0
0.45	0.2400	0.1832	0.2400	0.1151	5.78	805.0
0.50 ($y\to\infty$)	0.2375	0.1827	0.2375	0.1138	5.75	1637
not rounded triangular section	0.2500	0.1770	0.2500	0.1170	6.05	8

VIII. Rapid Flow Observation——Froude Number and Flow Stability

Most analytical flow stability criteria have been derived for two-dimensional flow and indicate that unsteady flow conditions exist when the Froude unmber F, exceeds 1.5 and 2.0 By definition, the Froude number is the ratio of the normal velocity V_0 to the critical velocity in the channel section,

$$\text{or} \qquad F=\frac{V_0}{C} \qquad \cdots\cdots(44)$$

Referring again to Eq. (42):

$$\frac{2}{3}\frac{1.486}{\nu g}\frac{J_1\delta^{\frac{1}{2}}}{\rho^{\frac{1}{3}}}\frac{d\rho}{d\zeta}=\pm 1$$

which defines the transition point between steady flow and pulsating flow, after rearranging, it can be written as:

$$\frac{2}{3}\frac{1.486J_1b^{\frac{1}{2}}\rho^{\frac{2}{3}}}{\nu gD}\frac{\delta}{\rho}\frac{d\rho}{d\zeta}=\pm 1 \qquad \cdots\cdots(45)$$

By using Eqs. (3)′ and (9) for the expression of V_0 and C, respectively, Eq. (45) may be expressed as

$$\frac{V_0}{C}=\pm\frac{3}{2}\frac{\rho}{\delta}\frac{d\zeta}{d\rho} \qquad \cdots\cdots(46)$$

or $$F=\pm\frac{3}{2}\frac{\rho}{\delta}\frac{d\zeta}{d\rho} \quad \cdots\cdots(47)$$

Eq. (47) applies to instability along a forward characteristic if $\frac{d\zeta}{d\rho}>0$ and to instability along a backward characteristic if $\frac{d\zeta}{d\rho}<0$. Thus, Eq.(47) can be rewritten to indicate that unstable flow conditions will exist when

$$F>1.5\frac{\rho}{\delta}\left|\frac{d\zeta}{d\rho}\right| \quad \cdots\cdots(48)$$

For a two-dimensional channel (for instance, rectangular channel, where D=y),

$$\frac{\rho}{\delta}\left|\frac{d\zeta}{d\rho}\right|=1 \quad \cdots\cdots(49)$$

then Eq.(48) becomes simply

$$F>1.5 \quad \cdots\cdots(50)$$

The experiments of H. J. koloseus, M. ASCE, indicate that for a wide, hydraulically rough channel, the Froude number for instability varies from 1.56 to 1.64 as the resitance coefficient, f, varies from 0.10 to 0.03 This criterion results from a theoretical developmeut which assumes that the resistance coefficient varies with relative roughness. The instability criterion, $F>1.5$, based on the development herein assumes that the resistance coefficient is independent of the relative roughness.

IX. Discussion and Comparison.

In this section, a series of discussion and comparison are made from those seven design charts which have been plotted in section Ⅶ Fig. 5 to Fig. 11. In order to discuss and compare its stability aspect between each similar pair of sections, we shall now classify the above seven charts into the following four parts:

【A】 Trapezoidal sections of side slopes "$\frac{\sqrt{3}}{3}$ on 1" (the best hydraulic section and "1 on 1" (Fig. 5 and Fig. 9, respectively):

(a) The critical depth curve of each chart as reference, for the same value of $\zeta=6$, Fig.5 indicates $\zeta=0.86$ and Fig.9. indicates $\zeta=0.79$. Since $\zeta=\frac{y}{b}$ it means that for the same base width b, the former section may has greater depth y than the latter, or the critical depth turning from tranquil flow to rapid flow for the best hydraulic section (side slopes $\frac{\sqrt{3}}{3}$ on 1) is higher than the section with side slopes 1 on 1. In fact, we may get the same result for any other value of ζ.

(b) The palsating flow curve as reference, in both cases, select $\xi=6$ for ins tance, $\zeta=0.50$ and $\zeta=0.46$ in Fig.5 and Fig.9, respectively. This indicates also that the best hydraulic section has a higher depth than the section of slopes 1 on 1. This also means that the best section is less stable for

it turns from steady rapid flow to pulsating rapid flow quickly.

(c) Noting that $J=\frac{s^{\frac{1}{2}}b^{\frac{1}{6}}}{n}$, $\xi=1.486\alpha\rho^{\frac{2}{3}}J=$ (slope) J and $\xi=\frac{Q}{b^{\frac{5}{2}}}$, for$\xi>1$ (larger discharge), the critical flow curve in each chart has nearly equal J, but the value of J in Fig.5, is larger than that of Fig.9. For pulsating flow curve, J-value is also larger in Fig. 5 than that in Fig.9 for $\xi>0.5$ but in both cases, J increases with the value ξ.

From these phenomena, we conclude that the best hydraulic section need larger J, or larger S (steeper slope) to change the flow conditions, i.e. from tranquil flow to steady rapid flow and from steady rapid flow to pulsating rapid flow. Therefore, the best seetion has more head loss than the "1 on 1" section. But for small $\xi(\xi<0.5)$the slope of the sloped lines in the two charts are nearly equal. For nearly equal ξ, these charts indicate that Fig.5 has smaller J value. This means that for a small constant discharge Q, the best section has smaller J or turning to pulsating flow faster than the section "1 on1", and is more effective.

(d) By comparing Fig.5 and Fig.9 for $\xi>0.5$, Fig.5 has smaller tranguil flow region and larger pulsating rapid flow region than Fig.9, and in both cases, the steady rapid flow region are nearly equal. But when $\xi<0.5$ (small discharge), Fig.5 has larger steady rapid flow region than Fig. 9. From these we conclude that the best section is somewhat less stable.

【B】 Round-cornered rectangular section and non-rounded rectangular section.(Fig. 6.and Fig. 10 respectively):

(a) Consider the critical depth curve, when $\xi=5$, $\zeta=0.76$ and $\zeta=0.92$ in Fig.6 and Fig.10, respectively. Thus for constant Q, the critical depth of round-cornered section is lower than the square-cornered section. This indicates that the rounded section has larger interval of depth for tranquil flow region and therefore is more stable and is much effective.

(b) For pulsating flow curve, when $\xi=5,\zeta=0.47$ and $\zeta=0.46$ in Fig.6 and Fig. 10 respectively. For other values of ξ also get the same result. It means that the depth of turning from steady rapid flow to pulsating rapid flow. the rounded section is somewhat greater and has smaller interval of depth. Therefore the stability of the rounded section is somewhat reduced.

(c) By $J=\frac{S^{\frac{1}{2}}b^{\frac{1}{6}}}{n}$, and the base width b in both sections are somewhat different, but with power $\frac{1}{6}$, they reduce to nearly equal value. Therefore, for the same ξ, the value of J for both curves in Fig.6 is smaller than that of Fig.10, This concludes that the energy gradient of the rounded section is smaller and also the loss of head is reduced. Therefore, the flow in rounded section is more stable than the non-rounded section. But in the case of small discharge ($\xi<0.2$,), J values of both sections

are nearly the same.

【C】Parabolic section and semicircular section (Fig.7 and Fig.11, respectively).: Of all poen-channel cross sections having a given area, the semicircle has the smallest wetted perimeter, and it is therefore the cross section of highest hydraulic efficiency. Escoffier and Boyd have derived a design chart for circular section and was copied in Fig. 11. In the case of semicircular section, $\zeta \leq 0.50$, and $y=\frac{T}{2}$, In Fig. 11, the author used dot-lines to represent the upper semicircle for $\zeta > 0.50$ and full-lines the required lower semicircle corresponding to $\zeta \leq 0.50$. We compare and discuss the parabolic and semicircular sections as follows.

(a) Critical depth curve as reference, when $\xi=1$, $\zeta=0.48$ in Fig.7 and $\zeta=0.42$ in Fig. 11. This shows that the critical depth of parabolic section is higher than the semicircular section. But for pulsating flow curve, if we choose again $\xi=1$ $\zeta=0.24$ in Fig. 7 and $\zeta=0.26$ in Fig. 11, it is just opposite to the former case and the depth of flow from steady rapid to pulsating rapid, the parabolic section is somewhat smaller.

(b) From above phenomena, we conclude that for a given discharge Q, the depth interval of tranguil flow for the parabolic section is smaller than the semicircle, but the interval of steady rapid flow is lower and turning to pulsating rapid flow region later than the semicircular section. This shows that the parabolic section is more stable and much effective than the semicircular section.

(c) In a parabolic section, when $\xi=0.25$, both curves have minimum value of J (critical depth curve, $\zeta=0.22$; pulsating flow curve, $\zeta=0.11$). For the other ξ, J values increase rapidly as ξ varied. This indicates that the hydraulic gradient of this section is steeper and the loss of head would be larger than the semicircular section.

(d) In parabolic section (Fig.7), ζvalues are plotted from 0.02 to 1.58, but semicircular section (Fig.11), the greatest ζ value is 0.50. Thus for large Q in tranquil flow, the parabolic section is much more effective than the circular one.

【D】Round-bottomed triangular section. (Fig. 8):

(a) Since $\zeta=\frac{y}{b}=\frac{y}{T}$ (b=T in this case), the unrounded triangular section has unique ζ value for they have the same ratio of y to T. When the intersecting angle $\theta=90°$, $\zeta=0.50$. For the rounded section, ζ has different value for different y. Thus when y is small, since the bottom is rounded, so that ζ varies quickly as y increases uniformly. But for large y, ζ will approach the limiting value 0.5 and when $y\to\infty$, $\zeta=0.5$.

(b) By $\xi=1.486\ \alpha\rho^{\frac{2}{3}}J$, $\text{slope}=1.486\alpha\rho^{\frac{2}{3}}$, the computed slopes for $\zeta=0.02\sim0.50$ are so closely that the design chart is very difficult to construct. In Fig.

8, the author constructed in two portions, including a complete critical depth curve and a segment of pulsating flow curve, instead of a complete design chart. From Table 4 cr the small chart in the upper-left corner of Fig. 8, the critical depth curve is very short and for each ζ, the value of J is approach to the definite number 6. Whereas the pulsating flow curve, the slope is very close to the slopping line of each ζ, and the variation of the curve for J values varying from 330 to 410 are plotted in the major part of Fig.8. The lower part is belong to the steady rapid flow region and the upper part is the pulsating rapid flow region.

(c) In the case of 90° V-shape channel (unrounded 90° triangular section, or $\mu=0$ in $r=\mu y$), the slopped-line in ξ-J diagram which computed directly from those parameters is approximately coincide with the line of $\zeta=0.35$ and is also represented in this chart.

(d) The critical flow curve in this chart indicates that the critical flow occurs only at the interval $\xi=0.58\sim0.66$, or $Q=0.58\,T^{\frac{5}{2}}\sim0.66T^{\frac{5}{2}}$, since $\xi=\frac{Q}{b^{\frac{5}{2}}}=\frac{Q}{T^{\frac{5}{2}}}$ (b=T in this section), J values (J_c) are ranging from 5.75 to 6.05, and is similar to the sections of trapezoid and round-cornered rectangle. Whereas the pulsating flow curve, J values (J_1) are starting from 165.4 when $\zeta=0.02$ to 1637.0 when $\zeta=0.50$ and for the ordinary triangular section (unrounded), $J_1\rightarrow\infty$. These indicate that the tranquil flow of the rounded section is nearly the same as the other sections, but the steady rapid flow region is larger. Besides, for the unrounded section, $J_1\rightarrow\infty$, it means that near the end of the steady flow region, the energy loss would be very large and the efficiency is very much reduced. But in the case of the rounded section, the energy or head loss would be smaller and increases rapidly as the value of ζ increases.

X. Conclusion:

(a) Four design charts have been derived by the author as shown in Figs. 5, 6, 7 and 8, are provided for use by engineers concerned with the hydraulics of open channels.

(b) These charts not only serve as a graphical determination of the type of flow existing in a channel, but also contribute to a better understanding of the phenomena involved in the flow.

(c) For trapezoidal channel sections, the section with flatter side slopes has smaller head loss and is also more stable than the one having steeper side slopes for an ordinary discharge. But in the case of small discharge, $\zeta<0.5$ or $Q<0.5\ b^{2.5}$ (cfs), the best trapezoidal section seems somewhat more effective (with small head loss) than the others.

(d) For rectangular channel sections, the round-cornered section has smaller energy loss and thus more efficient than the square-cornered section (

unrounded, i.e. r=0). In the flow of high stage, the rounded section is much more stable than the unrounded one, but in low stage, the rounded section is somewhat less effective. In general, we may adopt the round-cornered section to reduce its energy loss and also to increase its stability in ordinary stage of flow. Furthermore, the designer will be better to make the rounding radius r as large as possible.

(e) Between parabolic and semicircular sections, the former has larger depth interval of steady rapid flow zone but smaller interval in tranquil flow zone than the latter. Therefore, in high stage flow the parabolic section is more efficient, and in low stage flow the semicircular section is more efficient. Besides, the semicircular section has smaller head loss than the parabolic section, but the depth of the latter one can be increased continuously without limit. From these, we conclude that the parabolic section may be used with high efficiency in the case of high stage flow.

(f) For triangular sections, the round-bottomed section has smaller energy loss than the unrounded section. The steady rapid flow zone is also larger than other sections such as parabolic and rounded or unrounded rectangular sections. It can be used effectively in the flow of smaller discharge and the rounding radius r is also made as large as possible. The plotted chart (Fig. 8) can not be used in actual design, but it serves as a guide in examinning the flow nature and the characteristics of the rounded and unrounded rectangular sections.

(g) This study is due to analytical derivation and therefore, is a way of theoretical approach. But in the similar study which was proposed by Escoffier and Boyd in Nov. 1962, had been checked by a series of prototype tests on the Fort Randall spillway chute in June 1960 and also at the laboratory of the State University of Iowa. In fact, the theory and method of these two studies are the same, therefore the analysis and the final results of the present study will be valid in the same way.

REFERENCES

(1) "Stability aspects of Flow in Open Channels", by Francis F. Escoffier and Marden B. Boyd—Journal of the Hydraulics Division, Proceedings of ASCE, Vol.88, No. HY6, Nov.1962, Part I. P.P.145~166.

(2) Tables of Integrals and other Mathematical Data—by Herbert Bristol Dwight. (Third Edition).

(3) Discussion by F.F. Escoffier of "Roll Waves and Slug Flows in Inclined Open Channels,"—by P.G. Mager, Transactions, ASCE, Vol.126, Part I. 1961, p. 535.

(4) "A Graphical Method for Investigating the stability of Flow in Open Channels or in Closed Conduits Flowing Full,"—by F.F. Escoffier, Transactions, Amer. Geophysical Union, Vol.31, No.4 Aug.1950.

(5) Open-Channel Hydraulics—by Ven Te Chow, 1959, Chapt.18 p.p. 525~553.

(6) Advanced Calculus—by Watson Fulks, 1961. p.p. 219~221.
(7) Advanced Engineering Mathematics—by Erwin Kreyszig, 1962. p.p.304~369.
(8) Fluid Mechanics—by Richard H.F. Pao, 1961, Sect.11-6. p.p. 460~462.

各種不同斷面之渠道穩定分析及其研討

何 智 武*

摘 要

Francis F. Escoffier 及Marden B. Boyd 兩氏於 1962 年在美國土木工程師學會會報 (Proceedings of ASCE, "Journal of the Hydraulics Division," Vol.88, No. HY6. Nov. 1962, Part I) 上發表，曾採用三組參變數以分析矩形、梯形及圓形各種斷面渠道之穩定性，並繪製上述各種斷面之圖表，以供渠道設計者之參考。

又據L. Prandtl 氏之研究，在渠道斷面中，方角之斷面所產生之次水流 (Secondary flow) 較圓角之斷面 (Round-cornered section) 爲大，因此其能量之損失亦大。筆者據此提示，乃就常用之矩形及三角形兩種渠道斷面，將底部方角處改爲圓角，並加拋物線斷面及最高效率之梯形斷面，一共四種，仿 Escoffier 及 Boyd 兩氏之方法分析，並繪製該四種斷面之圖表，以供設計者使用，並可判斷各種水位之流狀及其穩定性。最後又將筆者所描製之各圖表與上列兩氏所描製之部分圖表兩者在損頭、流狀及穩定各方面作一詳盡之研討，以比較及研判各種圓角斷面在效果上之優劣。

誌 謝

本文得五十六年度國家長期發展科學委員會之補助，並承恩師理工學院沈院長百先和土木系姜主任子騅之鼓勵及指正，謹此誌謝。又土木四林亞祥同學協助描繪圖表，一併深致謝意。

*省立中興大學理工學院土木工程學系講師